ACS Photonics

Letter

pubs.acs.org/journal/apchd5

Digitalized Geometric Phases for Parallel Optical Spin and Orbital Angular Momentum Encoding

Peng Chen,[‡] Shi-Jun Ge,[‡] Wei Duan, Bing-Yan Wei, Guo-Xin Cui, Wei Hu,* and Yan-Qing Lu*

National Laboratory of Solid State Microstructures, College of Engineering and Applied Sciences, and Collaborative Innovation Center of Advanced Microstructures, Nanjing University, Nanjing 210093, China

Supporting Information

ABSTRACT: Geometric phases have attracted considerable attention in recent years, due to their capability of arbitrary beam shaping in a most efficient and compact way, while traditional geometric phases are usually limited to handling single-structured beams and lack the capability of parallel manipulation. Here, we propose a digitalized geometric phase enabling parallel optical spin and orbital angular momentum encoding. The concept is demonstrated in inhomogeneous anisotropic media by imprinting a particularly designed binary phase into a space-variant geometric phase. We theoretically analyze its spin−orbit interaction of light and experimentally created higher-order Poincaré sphere beam lattices, the order number and symmetry of which can be flexibly manipulated. Special lattices of cylindrical vector beams and orbital angular momentum modes with square and hexagonal symmetry are presented. This work discloses a new insight in programming geometric phases for tailoring the optical field and inspires various photonics applications.

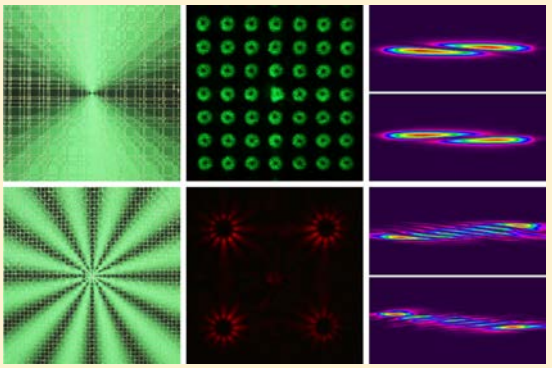

KEYWORDS: *higher-order Poincaré sphere, liquid crystal, geometric phase, orbital angular momentum, vector beam*

Light, as an excellent carrier of information, has been widely applied in modern communications. Due to the infinite number of orbital angular momentum (OAM) states of an optical vortex (OV), the capacity of optical communications systems can be drastically enhanced via OAM-based multiplexing and demultiplexing technology.[1−3] In addition, another mode-division multiplexing technique employing spatial polarization modes, i.e., cylindrical vector beams (CVBs),[4] is proved as a promising candidate as well.[5] Recently, the higher-order Poincaré (HOP) sphere has been introduced to geometrically describe the higher-order polarization states of these generalized vector vortex beams.[6,7] As is known, a traditional Poincaré sphere depicts all the polarization states of spatially homogeneous light. The poles represent the optical spin angular momentum (SAM) eigenstates, while for a HOP sphere, as shown in Figure 1, the north/south pole indicates right/left circularly polarized OV, which possesses a helical phase structure of $e^{\pm im\phi}$ and an OAM of $\pm m\hbar$,[8] where m is the topological charge. These two eigenstates incorporate both SAM and OAM, and each point on the HOP sphere is a linear superposition of them.[7] Especially, the equator of the HOP sphere represents the CVBs, featured by spatially variant polarization states, such as azimuthal and radial polarization. The phase or polarization singularity in the beam center results in a consistent donut-like intensity distribution. Besides optical communications, the HOP sphere beams have great potentials in optical manipulation, high-resolution imaging, and quantum informatics.[4,9] So far, two major strategies have been employed for HOP sphere beam generation. One is an interferometric approach through a modified Mach−Zender interferometer,[7] and the other is based on geometric phase elements.[10,11]

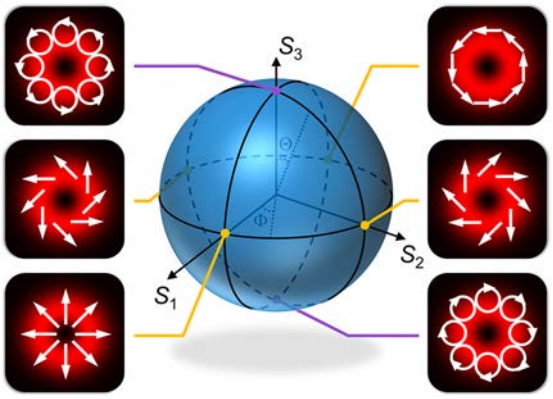

Figure 1. Schematic presentation of the HOP sphere with m = 1. Intensity distributions at certain points are shown with corresponding polarization distributions depicted by the white arrows. Θ and Φ are the spherical coordinates.

A geometric phase, also referred to as a Pancharatnam−Berry phase,[12] originates from the spin−orbit interaction of light,[13] which describes the coupling between the polarization and the

Received: March 16, 2017

ACS Publications © XXXX American Chemical Society

DOI: 10.1021/acsphotonics.7b00263
ACS Photonics XXXX, XXX, XXX−XXX

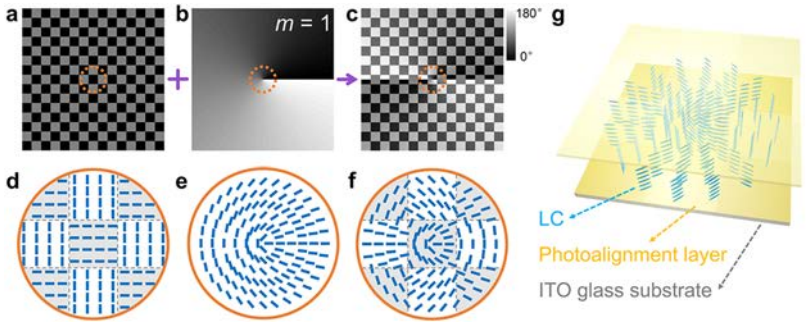

Figure 2. Optical axis distributions of (a and d) a 2 × 2 DG, (b and e) a *q*-plate with $m = 1$, and (c and f) corresponding integrated DQP. The color variation from black to white indicates the axis varying from 0° to 180°, and the blue sticks denote the local optical axis orientations in central regions. (g) Schematic cell configuration of the LC DQP.

trajectory of light and leads to spin-dependent light splitting, namely, the photonic spin Hall effect.[14] Unlike the dynamic phase, which arises from optical path differences, the geometric phase is associated with the space-variant manipulation of the light polarization state and depends only on the geometrical characteristics. Usually, its magnitude is proportional to the orientation angle of the effective local optical axis and has a polarization-dependent sign. It can be created from inhomogeneous anisotropic media, such as liquid crystals (LCs)[15,16] and anisotropic scatterer-based metasurfaces.[17−19] Via these physically thin geometric phase elements (usually working as half-wave plates), arbitrary wavefront shaping can be realized, such as spin-controlled focus/defocus,[20,21] diffraction,[22] and especially vortex and vector beam generation.[23−30]

Traditional geometric phases are usually limited to handling single-structured beams and lack the capability of parallel manipulation. If this challenge could be overcome, it would drastically extend the understanding and programming of geometric phases for structured beam tailoring and promote novel applications. For instance, the creation of HOP sphere beam arrays would inspire multiple optical tweezers,[31] parallel laser fabrication, and higher-efficiency stimulated emission depletion microscopy.[32] In this work, we digitalize a traditional space-variant geometric phase by imprinting a particular binary phase referring to binary optics and demonstrate the design in LCs by a dynamic photopatterning technique. With such digitalized geometric phase elements, HOP sphere beam lattices available for SAM and OAM parallel encoding are created for the first time. Via tuning the incident spin state, any point on the HOP sphere can be achieved, including special cases of CVBs and OAM modes. Square as well as hexagonal lattices with different desired orders are realized in high efficiency and good energy uniformity.

DESIGN AND PRINCIPLE

Dammann gratings (DGs) in binary optics can provide an equal-energy distribution among all desired diffraction orders,[33] thus supplying a promising strategy for parallel beam generation and manipulation. Each period of a DG is composed of certain binary phase (0 and π) regions with different widths.[34−36] The transmission function of a one-dimensional DG in the x direction can be described as[2]

$$T(x) = \exp(\mathrm{i}\varphi_{\mathrm{DG}}(x)) = \sum_{n=-\infty}^{+\infty} C_n \exp(\mathrm{i}2\pi x n/\Lambda) \tag{1}$$

where $\varphi_{\mathrm{DG}}(x)$ is the phase function of a DG, Λ is the period, and the coefficient C_n of the nth order can be expressed as[36]

$$C_n = \begin{cases} \dfrac{-\mathrm{i}}{2n\pi}\left[1 + 2\sum_{k=1}^{N-1}(-1)^k \exp(-\mathrm{i}2\pi n x_k) + (-1)^N \exp(-\mathrm{i}2\pi n x_N)\right] & n \neq 0 \\ 2\sum_{k=1}^{N-1}(-1)^k x_k + (-1)^N x_N & n = 0 \end{cases} \tag{2}$$

where $\{x_k\}$ are normalized phase transition points in each period with boundary values $x_0 = 0$ and $x_N = 1$, and N is the total number of transition points. $|C_n|^2$ is the power of the nth order normalized with respect to the total power. By optimizing the values and number of $\{x_k\}$, the incident light can be equally distributed into M desired orders in high efficiency. Via integrating two orthogonal one-dimensional DGs, i.e., $\varphi_{\mathrm{DG}} = \mathrm{mod}(\varphi_{\mathrm{DG}}(x) + \varphi_{\mathrm{DG}}(y), 2\pi)$, two-dimensional DGs could be obtained and have the ability to create $M_x \times M_y$ rectangular lattices. Diffractions with hexagonal lattices are achievable as well through integrating three one-dimensional DGs at a 60° angle to each other. Actually, the order number and symmetry of beam lattices can be arbitrarily manipulated by rationally predesigning the Dammann parameters.

Here, we introduce such a Dammann concept to digitalize traditional geometric phases, the spiral geometric phase of the *q*-plate[15] for instance. The designed optical axis orientation α follows the equation

$$\alpha = \frac{1}{2}m\phi + \frac{\varphi_{\mathrm{DG}}}{2} + \alpha_0 \tag{3}$$

where m denotes the topological charge, $\phi(x,y) = \arctan(y/x)$ is the azimuthal angle, and α_0 is the initial angle and usually assumed to be zero. In eq 3, the first term describes a *q*-plate, while the second term describes a DG. So we name it a Dammann-*q*-plate (DQP). As an example, Figure 2 illustrates the optical axis distributions of a 2 × 2 DG (normalized phase transition point: $x_1 = 0.5$), a *q*-plate with $m = 1$ and

DOI: 10.1021/acsphotonics.7b00263
ACS Photonics XXXX, XXX, XXX−XXX

corresponding integrated DQP, respectively. The color variation from black to white indicates the axis varying from 0° to 180° continuously, and the blue sticks denote the local optical axis orientations in central regions.

The property of the spin−orbit interaction induced diffraction can be theoretically predicted through Jones matrix calculation.[37] For a half-wave plate (HWP) with α with respect to the x axis, the Jones matrix is

$$\mathbf{J} = \begin{bmatrix} \cos(2\alpha) & \sin(2\alpha) \\ \sin(2\alpha) & -\cos(2\alpha) \end{bmatrix} \tag{4}$$

Consider an incident beam with arbitrary polarization:

$$|u_{in}\rangle = \cos\left(\frac{\Theta}{2}\right)e^{-i\Phi/2}|L\rangle + \sin\left(\frac{\Theta}{2}\right)e^{i\Phi/2}|R\rangle \tag{5}$$

where Θ and Φ are the spherical coordinates of a traditional Poincaré sphere and $|L\rangle = \frac{1}{\sqrt{2}}\begin{pmatrix}1\\ i\end{pmatrix}$ and $|R\rangle = \frac{1}{\sqrt{2}}\begin{pmatrix}1\\ -i\end{pmatrix}$ represent left and right circular polarization, respectively. The output light can be represented as

$$\begin{aligned} |u_{out}\rangle &= \mathbf{J}|u_{in}\rangle \\ &= \cos\left(\frac{\Theta}{2}\right)e^{-i\Phi/2}|R\rangle e^{i2\alpha} + \sin\left(\frac{\Theta}{2}\right)e^{i\Phi/2}|L\rangle e^{-i2\alpha} \\ &= \left[\cos\left(\frac{\Theta}{2}\right)e^{-i\Phi/2}|R_m\rangle + \sin\left(\frac{\Theta}{2}\right)e^{i\Phi/2}|L_{\bar{m}}\rangle\right]e^{i\varphi_{DG}} \\ &= \sum_{n_x=-\infty}^{+\infty}\sum_{n_y=-\infty}^{+\infty} C_{n_x}C_{n_y}\exp(i2\pi x n_x/\Lambda_x)\exp(i2\pi y n_y/\Lambda_y)|u_m\rangle \end{aligned} \tag{6}$$

where $\pm 2\alpha$ is the geometric phase induced by spin−orbit interaction of light and $|R_m\rangle = |R\rangle e^{im\phi}$ and $|L_{\bar{m}}\rangle = |L\rangle e^{-im\phi}$ are precisely the two eigenstates of the HOP sphere, and their linear superposition $|u_m\rangle = \cos\left(\frac{\Theta}{2}\right)e^{-i\Phi/2}|R_m\rangle + \sin\left(\frac{\Theta}{2}\right)e^{i\Phi/2}|L_{\bar{m}}\rangle$ is exactly the description of any point on the HOP sphere.[7,11] On the other hand, the DG term contributes to an equal-energy array. In all, the incident light will be equally diffracted into desired orders with a certain state of the HOP sphere controlled by the incident polarization.

Due to the pronounced large optical anisotropy and the controllable continuously variant director (i.e., local optical axis) distribution, LCs become the first choice for demonstrating a DQP. An LC is a natural birefringent material, and the refractive index difference will result in phase retardation:

$$\Gamma = \frac{2\pi(n_{eff} - n_o)d}{\lambda} \tag{7}$$

where d is the LC cell gap, λ is the wavelength of the incident light, and n_{eff} is the effective extraordinary refractive index, which changes from n_e to n_o with increasing voltage due to the tilting of LC molecules.[38] By particularly choosing the refractive indices of LCs and the cell gap, or applying specific voltages to reach $\Gamma = (2a + 1)\pi$ (a is an integer), it could work as a half-wave plate. Moreover, LCs are highly stable and commercially available and have roughly no absorption in the visible band.

The schematic cell configuration of the LC DQP is presented in Figure 2g, whose director distribution follows eq 3 and is consistent with Figure 2f. The photoalignment technique has been proved very suitable for high-resolution multidomain LC alignments.[39] Here, sulfonic azo-dye SD1, a polarization-sensitive and rewritable alignment agent, was adopted. SD1 molecules tend to reorient perpendicular to the polarization direction of illuminated UV light and then guide the LC directors.[40] Two pieces of indium−tin-oxide (ITO) glass substrates spin-coated with SD1 were assembled with 6 μm spacers and then sealed with epoxy glue to form the cell. A multistep partly overlapping exposure process was performed to carry out the designed structures through a digital micromirror device based dynamic microlithography system,[28,41] the detailed process of which can be found in the Supporting Information. Afterward, filling the cell with nematic LC E7 yielded the proposed DQPs.

RESULTS AND DISCUSSION

Figure 3a exhibits a micrograph of a 2 × 2 DQP with m = 1, corresponding to Figure 2c. The continuous varying of the director leads to a continuous change of the brightness. Compared to conventional q-plates, net-like disclinations consistent with the structure of an encoded 2 × 2 DG shown in Figure 2a are observed. It is caused by the 90° shift of the LC director astride the discontinuities. These indicate that the desired optical axis distribution has been faithfully realized in the LC layer. The experimental optical setup for generating and analyzing HOP sphere beam lattices is illustrated in Figure 3j. The first polarizer and quarter-wave plate (QWP) or HWP are used to control the incident polarization of a 632.8 nm laser. Another polarizer is utilized to analyze the output polarization. The diffraction patterns are captured by a camera. To verify the topological charges of resultant OAM modes, the astigmatic transformation method[42] is adopted by inserting a cylindrical lens (f = 100 mm) in front of a CCD. A voltage of 2.5 V is applied to the LC cell to keep the half-wave condition.

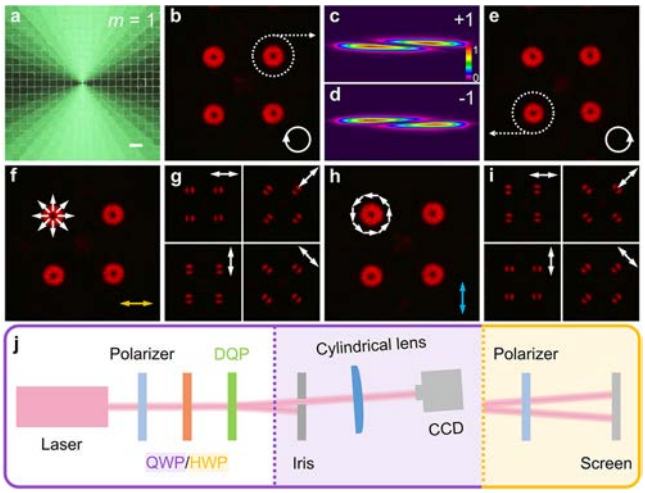

Figure 3. (a) Micrograph of the 2 × 2 DQP with m = 1 recorded under a polarized optical microscope. The scale bar is 100 μm. Diffraction patterns at 632.8 nm with different incident polarization: (b) left and (e) right circular polarization with corresponding OAM detection shown in (c) and (d), respectively, (f) horizontal and (h) vertical linear polarization with (g) and (i) after transmission through a rotating analyzer labeled by double-ended arrows. (j) Experimental optical setup.

DOI: 10.1021/acsphotonics.7b00263
ACS Photonics XXXX, XXX, XXX−XXX

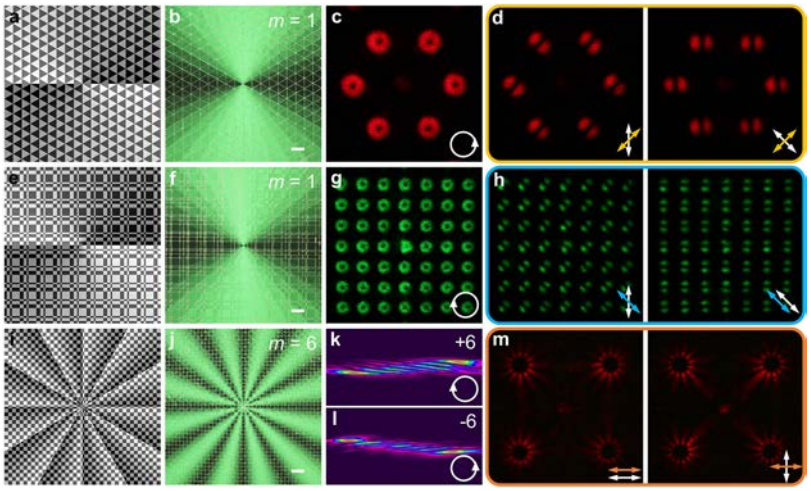

Figure 4. Designed optical axis distributions and micrographs of (a, b) a hexagonal DQP with $m = 1$, (e, f) a 7 × 7 DQP with $m = 1$, and (i, j) a 2 × 2 DQP with $m = 6$, respectively. All scale bars are 100 μm. Diffraction patterns of samples in (b) and (f) with (c) right and (g) left circular incident polarization. One of the generated OAM modes of the sample in (j) is converted by the cylindrical lens with (k) left and (l) right circular incident polarization. (d, h, and m) Diffraction patterns of samples in (b), (f), and (j), respectively, with different directions of the polarizer and analyzer indicated by double-ended arrows.

As expected, for $|u_{in}\rangle = |L\rangle$, a 2 × 2 square lattice of donut-like OVs with right circular polarization is obtained, as shown in Figure 3b. Figure 3c reveals the converted pattern of one such OV captured in the focal plane of the cylindrical lens. The number of dark stripes and the stripe tilt direction[42] indicate the topological charge of +1. That means a 2 × 2 square lattice of the beam on the north pole of the HOP sphere ($|R_{+1}\rangle$) is created, while for $|u_{in}\rangle = |R\rangle$, a 2 × 2 lattice of $|L_{-1}\rangle$ is generated as presented in Figure 3e and d. For $|u_{in}\rangle = \frac{1}{\sqrt{2}}[|L\rangle + |R\rangle]$, a radial polarization ($\frac{1}{\sqrt{2}}[|R_{+1}\rangle + |L_{-1}\rangle]$) is obtained (Figure 3f) with the lobed structures parallel to the orientation of the rotating analyzer (Figure 3g). Similarly, the square lattice of the azimuthal polarization ($\frac{i}{\sqrt{2}}[-|R_{+1}\rangle + |L_{-1}\rangle]$) is also achieved with $|u_{in}\rangle = \frac{i}{\sqrt{2}}[-|L\rangle + |R\rangle]$, and the lobed structures are perpendicular to the orientation of the analyzer, as shown in Figure 3h and i. Beam lattices of other points on the HOP sphere could also be produced via SAM control.[11] Furthermore, the diffraction efficiency (η, defined as the intensity ratio of the objective diffraction order to the total transmitted light) is measured for all four main orders. η is equal to 16.2%, 16.1%, 16.2%, and 16% (±0.2%), respectively. The total efficiency is η = 64.5% (±0.5%), consistent with the theoretical value 65.6% (81% × 81%).[34] These results verify the good energy uniformity and high efficiency.

In addition to square lattices, a hexagonal lattice of the HOP sphere beam is also demonstrated by encoding the phase of three one-dimensional DGs (60° to each other, $x_1 = 0.5$) into a spiral geometric phase with $m = 1$. The corresponding optical axis distribution is exhibited in Figure 4a, and the micrograph is shown subsequently. For circular incident polarization, a hexagonal lattice of orthogonal circularly polarized OAM modes is generated as shown in Figure 4c, while for linear incident polarization, hexagonal lattices of CVBs are obtained, with an example of $|u_{in}\rangle = \frac{1}{\sqrt{2}}[e^{-i\pi/4}|L\rangle + e^{i\pi/4}|R\rangle]$ presented in Figure 4d. Via choosing proper phase transition points within each period, it is possible to obtain more orders. For example, seven desired diffraction orders correspond to $x_1 = 0.23191$, $x_2 = 0.42520$, and $x_3 = 0.52571$.[34] A 7 × 7 DQP with $m = 1$ is fabricated with an optical axis distribution and the micrograph revealed in Figure 4e and f, respectively. By electrical tuning, the phase retardation can reach π at different wavelengths, making the LC DQP wavelength tolerant. According to eq 7, for a shorter wavelength, the operation voltage should be increased to make Γ satisfy the half-wave condition. For instance, at 2.7 V, an equivalent diffraction property is also achieved at 532 nm, as shown in Figure 4g and h. The analysis for the general condition can be found in the Supporting Information. Besides, the electro-optical tunability of LCs makes it possible to dynamically switch between *on*/*off* states.[36] Furthermore, square lattices of a HOP sphere with a larger topological charge $m = 6$ are created. More bright-to-dark alternations can be observed in Figure 4j. For OAM detection in Figure 4k and l, the number of dark stripes is six, consistent with its topological charge. The generated CVB arrays are exhibited in Figure 4m, featuring 12 lobes after transmission through the analyzer.

CONCLUSION

In conclusion, the flexible creation of HOP sphere beam lattices for parallel SAM and OAM encoding is presented through digitalized geometric phases, which are demonstrated in LCs and carried out by photoalignment technology. An arbitrary state on the HOP sphere can be obtained, including the special cases of CVBs as well as OAM modes. Both square and hexagonal HOP sphere beam lattices with different desired orders and topological charges are realized in high efficiency and good energy uniformity. In addition, merits of high quality, electrical switchability, and tolerance to the wavelength of incident light are exhibited. This idea, not restricted to a Dammann encoded spiral geometric phase, can be extended to other integrations of binary phases and space-variant geometric phases, permitting the realization of versatile optical beam tailoring. Actually, the medium is not limited to LCs. Other natural or artificial birefringent materials are adoptable as well. This work may provide a brand new idea in programming geometric phases and brings extra opportunities to optical

DOI: 10.1021/acsphotonics.7b00263
ACS Photonics XXXX, XXX, XXX−XXX

communications, laser fabrication, super-resolution imaging, etc.

■ ASSOCIATED CONTENT

Supporting Information

The Supporting Information is available free of charge on the ACS Publications website at DOI: 10.1021/acsphotonics.7b00263.

Fabrication process and general conditions for the LC DQP (PDF)

■ AUTHOR INFORMATION

Corresponding Authors

*E-mail: huwei@nju.edu.cn.

*E-mail: yqlu@nju.edu.cn.

ORCID

Wei Hu: 0000-0003-1255-9453

Author Contributions

‡P. Chen and S. J. Ge contributed equally to this work.

Notes

The authors declare no competing financial interest.

■ ACKNOWLEDGMENTS

This work was supported by the National Natural Science Foundation of China (NSFC) (Nos. 61490714, 61435008, 61575093, 11304151, and 11604144).

■ REFERENCES

(1) Wang, J.; Yang, J. Y.; Fazal, I. M.; Ahmed, N.; Yan, Y.; Huang, H.; Ren, Y. X.; Yue, Y.; Dolinar, S.; Tur, M.; Willner, A. E. Terabit free-space data transmission employing orbital angular momentum multiplexing. *Nat. Photonics* **2012**, *6*, 488−496.

(2) Lei, T.; Zhang, M.; Li, Y.; Jia, P.; Liu, G. N.; Xu, X.; Li, Z.; Min, C.; Lin, J.; Yu, C.; Niu, H.; Yuan, X. Massive individual orbital angular momentum channels for multiplexing enabled by dammann gratings. *Light: Sci. Appl.* **2015**, *4*, e257.

(3) Willner, A. E.; Huang, H.; Yan, Y.; Ren, Y.; Ahmed, N.; Xie, G.; Bao, C.; Li, L.; Cao, Y.; Zhao, Z.; Wang, J.; Lavery, M. P. J.; Tur, M.; Ramachandran, S.; Molisch, A. F.; Ashrafi, N.; Ashrafi, S. Optical communications using orbital angular momentum beams. *Adv. Opt. Photonics* **2015**, *7*, 66−106.

(4) Zhan, Q. Cylindrical vector beams: from mathematical concepts to applications. *Adv. Opt. Photonics* **2009**, *1*, 1−57.

(5) Milione, G.; Lavery, M. P.; Huang, H.; Ren, Y.; Xie, G.; Nguyen, T. A.; Karimi, E.; Marrucci, L.; Nolan, D. A.; Alfano, R. R.; Willner, A. E. 4 × 20 Gbit/s mode division multiplexing over free space using vector modes and a q-plate mode (de) multiplexer. *Opt. Lett.* **2015**, *40*, 1980−1983.

(6) Milione, G.; Sztul, H.; Nolan, D.; Alfano, R. Higher-order Poincaré sphere, Stokes parameters, and the angular momentum of light. *Phys. Rev. Lett.* **2011**, *107*, 053601.

(7) Milione, G.; Evans, S.; Nolan, D.; Alfano, R. Higher order Pancharatnam-Berry phase and the angular momentum of light. *Phys. Rev. Lett.* **2012**, *108*, 190401.

(8) Allen, L.; Beijersbergen, M. W.; Spreeuw, R. J. C.; Woerdman, J. P. Orbital angular momentum of light and the transformation of Laguerre-Gaussian laser modes. *Phys. Rev. A: At., Mol., Opt. Phys.* **1992**, *45*, 8185−8189.

(9) Yao, A. M.; Padgett, M. J. Orbital angular momentum: origins, behavior and applications. *Adv. Opt. Photonics* **2011**, *3*, 161−204.

(10) Cardano, F.; Karimi, E.; Slussarenko, S.; Marrucci, L.; Lisio, C. D.; Santamato, E. Polarization pattern of vector vortex beams generated by q-plates with different topological charges. *Appl. Opt.* **2012**, *51*, C1−C6.

(11) Naidoo, D.; Roux, F. S.; Dudley, A.; Litvin, I.; Piccirillo, B.; Marrucci, L.; Forbes, A. Controlled generation of higher-order Poincaré sphere beams from a laser. *Nat. Photonics* **2016**, *10*, 327−332.

(12) Pancharatnam, S. Generalized theory of interference and its applications. *Proc. Ind. Acad. Sci. A* **1956**, *44*, 247−262.

(13) Bliokh, K.; Rodríguez-Fortuño, F.; Nori, F.; Zayats, A. V. Spin-orbit interactions of light. *Nat. Photonics* **2015**, *9*, 796−808.

(14) Yin, X.; Ye, Z.; Rho, J.; Wang, Y.; Zhang, X. Photonic spin Hall effect at metasurfaces. *Science* **2013**, *339*, 1405−1407.

(15) Marrucci, L.; Manzo, C.; Paparo, D. Optical spin-to-orbital angular momentum conversion in inhomogeneous anisotropic media. *Phys. Rev. Lett.* **2006**, *96*, 163905.

(16) Kim, J.; Li, Y.; Miskiewicz, M. N.; Oh, C.; Kudenov, M. W.; Escuti, M. J. Fabrication of ideal geometric-phase holograms with arbitrary wavefronts. *Optica* **2015**, *2*, 958−964.

(17) Yu, N.; Capasso, F. Flat optics with designer metasurfaces. *Nat. Mater.* **2014**, *13*, 139−150.

(18) Mei, S.; Mehmood, M. Q.; Hussain, S.; Huang, K.; Ling, X.; Siew, S. Y.; Liu, H.; Teng, J.; Danner, A.; Qiu, C. W. Flat helical nanosieves. *Adv. Funct. Mater.* **2016**, *26*, 5255−5262.

(19) Ling, X.; Zhou, X.; Huang, K.; Liu, Y.; Qiu, C. W.; Luo, H.; Wen, S. Recent advances in the spin Hall effect of light. *Rep. Prog. Phys.* **2017**, *80*, 066401.

(20) Hasman, E.; Kleiner, V.; Biener, G.; Niv, A. Polarization dependent focusing lens by use of quantized Pancharatnam-Berry phase diffractive optics. *Appl. Phys. Lett.* **2003**, *82*, 328−330.

(21) Ke, Y.; Liu, Y.; Zhou, J.; Liu, Y.; Luo, H.; Wen, S. Optical integration of Pancharatnam-Berry phase lens and dynamical phase lens. *Appl. Phys. Lett.* **2016**, *108*, 101102.

(22) Bomzon, Z. E.; Biener, G.; Kleiner, V.; Hasman, E. Space-variant Pancharatnam-Berry phase optical elements with computer-generated subwavelength gratings. *Opt. Lett.* **2002**, *27*, 1141−1143.

(23) Marrucci, L.; Manzo, C.; Paparo, D. Pancharatnam-Berry phase optical elements for wave front shaping in the visible domain: switchable helical mode generation. *Appl. Phys. Lett.* **2006**, *88*, 221102.

(24) Huang, Y. H.; Ko, S. W.; Li, M. S.; Chu, S. C.; Fuh, A. Y. G. Modulation of shape and polarization of beam using a liquid crystal q-plate that is fabricated via photo-alignment. *Opt. Express* **2013**, *21*, 10954−10961.

(25) Karimi, E.; Schulz, S. A.; Leon, I. D.; Qassim, H.; Upham, J.; Boyd, R. W. Generating optical orbital angular momentum at visible wavelengths using a plasmonic metasurface. *Light: Sci. Appl.* **2014**, *3*, e167.

(26) Yue, F.; Wen, D.; Xin, J.; Gerardot, B. D.; Li, J.; Chen, X. Vector vortex beam generation with a single plasmonic metasurface. *ACS Photonics* **2016**, *3*, 1558−1563.

(27) Mehmood, M. Q.; Mei, S.; Hussain, S.; Huang, K.; Siew, S. Y.; Zhang, L.; Zhang, T.; Ling, X.; Liu, H.; Teng, J.; Danner, A.; Zhang, S.; Qiu, C. W. Visible-frequency metasurface for structuring and spatially multiplexing optical vortices. *Adv. Mater.* **2016**, *28*, 2533−2539.

(28) Ji, W.; Lee, C. H.; Chen, P.; Hu, W.; Ming, Y.; Zhang, L.; Lin, T. H.; Chigrinov, V.; Lu, Y. Q. Meta-q-plate for complex beam shaping. *Sci. Rep.* **2016**, *6*, 25528.

(29) Guo, Y.; Pu, M.; Zhao, Z.; Wang, Y.; Jin, J.; Gao, P.; Li, X.; Ma, X.; Luo, X. Merging geometric phase and plasmon retardation phase in continuously shaped metasurfaces for arbitrary orbital angular momentum generation. *ACS Photonics* **2016**, *3*, 2022−2029.

(30) Huang, L.; Song, X.; Reineke, B.; Li, T.; Li, X.; Liu, J.; Zhang, S.; Wang, Y.; Zentgraf, T. Volumetric generation of optical vortices with metasurfaces. *ACS Photonics* **2017**, *4*, 338−346.

(31) Grier, D. G. A revolution in optical manipulation. *Nature* **2003**, *424*, 810−816.

(32) Yan, L.; Gregg, P.; Karimi, E.; Rubano, A.; Marrucci, L.; Boyd, R.; Ramachandran, S. Q-plate enabled spectrally diverse orbital-angular-momentum conversion for stimulated emission depletion microscopy. *Optica* **2015**, *2*, 900−903.

(33) Dammann, H.; Klotz, E. Coherent optical generation and inspection of two-dimensional periodic structures. *Opt. Acta* **1977**, *24*, 505−515.

DOI: 10.1021/acsphotonics.7b00263
ACS Photonics XXXX, XXX, XXX−XXX

(34) Zhou, C.; Liu, L. Numerical study of Dammann array illuminators. *Appl. Opt.* **1995**, *34*, 5961−5969.
(35) Luo, D.; Sun, X. W.; Dai, H. T.; Demir, H. V. Polarization-dependent circular Dammann grating made of azo-dye-doped liquid crystals. *Appl. Opt.* **2011**, *50*, 2316−2321.
(36) Chen, P.; Ge, S. J.; Ma, L. L.; Hu, W.; Chigrinov, V.; Lu, Y. Q. Generation of equal-energy orbital angular momentum beams via photopatterned liquid crystals. *Phys. Rev. Appl.* **2016**, *5*, 044009.
(37) Yeh, P.; Gu, C. *Optics of Liquid Crystal Displays*; Wiley: New York, 1999.
(38) Khoo, I. C.; Wu, S. T. *Optics and Nonlinear Optics of Liquid Crystals*; World Scientific: Singapore, 1993.
(39) Schadt, M.; Seiberle, H.; Schuster, A. Optical patterning of multi-domain liquid-crystal. *Nature* **1996**, *381*, 212−215.
(40) Chigrinov, V.; Pikin, S.; Verevochnikov, A.; Kozenkov, V.; Khazimullin, M.; Ho, J.; Huang, D. D.; Kwok, H. S. Diffusion model of photoaligning in azo-dye layers. *Phys. Rev. E* **2004**, *69*, 061713.
(41) Chen, P.; Wei, B. Y.; Ji, W.; Ge, S. J.; Hu, W.; Xu, F.; Chigrinov, V.; Lu, Y. Q. Arbitrary and reconfigurable optical vortex generation: a high-efficiency technique using director-varying liquid crystal fork gratings. *Photonics Res.* **2015**, *3*, 133−139.
(42) Denisenko, V.; Shvedov, V.; Desyatnikov, A. S.; Neshev, D. N.; Krolikowski, W.; Volyar, A.; Soskin, M.; Kivshar, Y. S. Determination of topological charges of polychromatic optical vortices. *Opt. Express* **2009**, *17*, 23374−23379.

DOI: 10.1021/acsphotonics.7b00263
ACS Photonics XXXX, XXX, XXX−XXX